University of Thi-Qar Journal of Science (UTJsci)
E-ISSN: 2709-0256, P-ISSN: 1991-8690, Vol. 13, No. 1, Jun. 2026

Simplified Plasmonic Filter for Improved Optical Functionality

Anwar H. Nasser *[1a] and Hassan A. Yasser [1b]

[1] *Department of Physics, College of Science, University of Thi-Qar, Thi-Qar, Iraq.*

[b]E-mail: hassan.yasser@sci.utq.edu.iq
[a*]Corresponding author: Anwar.hasan@utq.edu.iq

Received: 2025-06-21, Revised: 2025-07-28, Accepted: 2025-08-10, Published: 2026-06-01

***Abstract*— In this paper, the behavior of a plasmonic filter structured around a metal-air-metal waveguide incorporating a washer-like resonator was investigated. The transmittance spectrum and magnetic field (Hz) distributions were analyzed using the finite element method (FEM) within the COMSOL Multiphysics software (version 6.0). The impact of various geometrical parameters-such as width of the washer (d), gap width (g), external radius of the washer, and material configuration on the optical characteristics of the filter including transmission, reflection, and absorption were thoroughly examined. Our results showed that enlarging the value of d led to a redshift in the transmission spectrum and strengthened the resonant interaction, whereas narrowing g weakened the optical coupling and shifted the spectrum toward the blue region. Hence, the observed spectral shifts and tunable features emphasized the filter's adaptability, which can be leveraged in various photonic and nano-optical platforms with minimal structural changes. We observed that the full width at half maximum (FWHM) and quality factor were significantly affected by the washer radius and structure length, highlighting the resonance resolution and transmittance efficiency. The proposed filter achieved transmission exceeding 70%, a quality factor of up to 70, and a bandwidth of 10 nm. These values were obtained at the resonance wavelength of 800 nm. Furthermore, comparing the results between silver and gold using the Drude model revealed that gold offered a lower transmission efficiency and quality factor comparing to silver. We did not focus on gold, as it has low absorbency, making it an ideal choice for high-performance optical filtering applications. These insights contributed to the advancement of tunable plasmonic systems used in fields like optical sensing and spectral filtering.**

***Keywords*— plasmonic filter, FWHM, Surface plasmon resonance, quality factor.**

I. INTRODUCTION

Plasmons are quasi-particles that represent the collective oscillations of free electrons in a metal. Surface plasmons (SPs) are confined to the metal-dielectric interface [1]. Surface plasmon polaritons (SPPs) are formed when light interacts with the electron cloud on a metal surface, allowing energy to propagate along the boundary between the metal and the dielectric. These waves are known for their ability to confine electromagnetic fields to extremely narrow spaces. Thanks to this strong field localization, SPPs have become valuable in applications ranging from nano-optics to sensing and signal processing [2]. The optical behavior of SPs can be adjusted by changing the size and shape of metal nanostructures, such as nanoparticles, nanorods, and nano disks. These geometric variations enable the tuning of resonance modes, allowing for flexibility in designing nanophotonic devices [3].

SPs may exist in various physical forms depending on the involved structure. Some SPs propagate freely along flat metal surfaces, while others are confined as localized oscillations within metal nanoparticles. This allows for transferring and controlling the energy at nanoscale and supporting the development of integrated plasmonic devices for optical and sensing applications [4].

Metal-insulator-metal (MIM) structures have demonstrated the ability to enhance surface sensitivity by supporting resonant modes tightly confined within the insulator gap. This confinement enables precise detection of refractive index changes, making these structures highly promising for advanced sensing and filtration applications [5]. MIM waveguides serve as foundational elements in nanophotonic circuits, allowing precise light manipulation at subwavelength scales. They are compatible with plasmonic devices, such as optical filters [6]. Furthermore, recent theoretical insights indicate that coupling split semi-circular ring resonators to MIM waveguides enables strong plasmonic coupling. This leads to enhance tunability and have sharper resonance modes, which is particularly advantageous for compact plasmonic filter designs addressing transmission selectivity and quality factor demands [7].

In modern optical systems, plasmonic filters based on MIM waveguides have become essential components for communications applications due to their ability to control specific transmission bands with high precision, efficiently separating and directing optical signals [8]. Plasmonic systems enable light-based signal transmission at speeds beyond conventional electronics [9]. The excitation of SPPs provides an efficient mechanism for channeling electromagnetic energy at nanometer dimensions. These tightly confined plasmonic waves can be modulated on ultrafast timescales. Studies have demonstrated the excitation of SPs at frequency ranges equivalent to terahertz, opening the door to data transmission rates up to terabits per second [3].

https://doi.org/10.32792/utq/utjsci/v13i1.1430

In optical communication systems, plasmonic filters are expected to play a pivotal role in improving the efficiency of WDM technologies by enabling accurate separation and direction of multiple optical signals. These filters allow for high-precision and selective wavelength discrimination in applications such as imaging and spectroscopy, which are crucial for modern analytical methods [10]. Moreover, their capability to function at elevated frequencies, spanning from the visible range to the near-infrared, expands their potential use across a wide spectrum of technological fields [10,11].

Noble metals (Au, Ag, Pt) are distinguished by unique properties such as resistance to corrosion and oxidation, unusually high reduction potential, non-reactiveness, high melting point, high ionization energy have attracted great interest of scientific community to design their functional nanoparticles for applied multiple. The physiochemical properties of noble metal nanoparticles are dictated by various attributes like size, shape, crystallinity, architecture and composition [13].

However, alongside these advantages, certain limitations-associate with the intrinsic losses arising from the use of metallic components in such filters [14]. Metals inherently exhibit absorption losses due to their limited electrical conductivity, which constrains the overall efficiency of plasmonic devices. researchers have begun investigating doped semiconductors and transparent conducting oxides (TCOs) such as aluminum-doped zinc oxide for plasmonic applications due to their lower intrinsic optical losses and tunable optical properties. Additionally, hybrid metal–insulator configurations have been explored to strike a balance between field confinement and energy dissipation, thereby improving overall device efficiency [15].

In recent years, plasmonic filters have been improved significantly , focusing on enhancing their spectral selectivity and reducing intrinsic losses associated with metallic components [16]. However, many existing designs face limitations in balancing filter compactness with transmission efficiency and quality factor [17]. The proposed design addressed these challenges by enabling tunable spectral response with fewer structural complexities, improving transmission efficiency while maintaining a high quality factor. Moreover, the comprehensive analysis of geometric parameters enhances the filter's design flexibility and offers valuable insights for researchers working on fiber-optic signal processing, a field currently gaining significant momentum.

II. PROPOSED STRUCTURE IN COMSOL ENVIRONMENT

The designed plasmonic filter comprises a metallic rectangular with dimensions L_1 and L_2. At the center of this metallic structure, a circular washer-shaped cavity is placed, defined by inner and outer radii r_1 and r_2, leaving a central metallic disc with radius r_1. Along the midline of the rectangle's width, two rectangular apertures with lengths L and widths W_1 were introduced at both ends of the structure. One apertures served as the input port and the other was the output for the electromagnetic waves.

Furthermore, a cross-section of a washer is cut at the top and bottom of the central pointer with radii r_3 and r_4, where $r_4 = r_3 + W_2$. This cross-section starts from an angle θ and ends at angle . The beginning of the first horizontal rectangle was chosen for the entry of electromagnetic waves and the end of the second rectangle is selected for the departure of these waves. The two rectangles, the central washer and the washer sectors around composed of air, while the remaining portions of the filter composed of a noble metal.

The separation between each horizontal rectangular port and the central washer is denoted by g, which is also the distance maintained between the central washer and the arc-shaped sectors at the top and bottom. Table (1) explains the simulation parameters and Fig.1; shows the structure of the proposed plasmonic filter. Note that, changing the filter parameters during the simulation will be noted in its place.

TABLE I. dimensions of the proposed structure.

parameter	Value	parameter	value
L	200nm	θ	35^o
L_1	$2L + 2r_3$	r_1	120nm
L_2	$2r_3 + 200nm$	r_2	$r_1 + d$
W_1	35nm	r_3	$r_2 + g$
W_2	40nm	r_4	$r_3 + W_2$
g	14nm	d	45nm

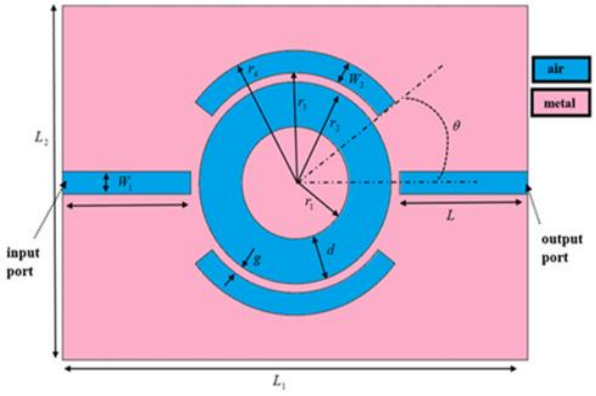

Fig: (1): the proposed structure filter.

To accurately model the optical properties of the noble metal used in the proposed plasmonic filter, the Drude model was employed. This model describes the frequency-dependent dielectric function of metals and is particularly suitable for capturing the free electron response in noble metals like gold and silver. The Drude model equation is given by [18]

$$\varepsilon = 1 - \frac{w_p^2}{w^2 + i\gamma w} \qquad (1)$$

Where: ε the dielectric function, w_p Plasma frequency of the metal, γ Damping factor, w: Angular frequency of the incident electromagnetic wave. In COMSOL Multiphysics, the material properties of noble metals are typically implemented using the Drude model, with predefined values for wp and γ depending on the selected metal (e.g., silver or gold).

III. Filter Metrics

In plasmonic platforms, the resonance frequency denotes the specific frequency when SPPs or localized surface plasmon resonances (LSPRs) are effectively triggered due to the coupling between incident electromagnetic waves and the oscillation of free electrons within the metal [19]. This frequency plays a fundamental role in determining the operational characteristics of plasmonic components such as waveguides, sensors, and filters. The performance of a plasmonic structure depends on a combination of the optical properties of its constituent material, the refractive properties of its surrounding environment, and its geometric configuration. Together, these factors influence key performance metrics, such as resonance efficiency, field confinement, and spectral sensitivity [20].

In plasmonic metal nanoparticles, resonance is highly dependent on its physical scale and architecture. For instance, adjusting the size or shaping of particles enables tuning of the resonant wavelength. Furthermore, selecting different metallic compositions can shift resonance's characteristics and changes in the refractive index of the surrounding medium lead to significant changes in the resonance's frequency, making plasmonic systems highly responsive in sensing applications. This resonance's frequency strongly influences how plasmonic devices perform in terms of filtering behavior and photonic interactions. It directly impacts energy absorption characteristics and determines the device's effectiveness in sensing applications [21].

The FWHM quantifies the spectral bandwidth occupied by a resonance at 50% of its peak intensity. A smaller FWHM indicates tighter spectral confinement, which translates to sharper resonance and higher color. This characteristic is especially valuable in plasmonic systems like narrow-band filters and high-resolution sensors, where it directly correlates with performance metrics such as the quality factor and overall detection sensitivity. FWHM can be calculated using the following formula:

$$FWHM = \lambda_2 - \lambda_1 \tag{2}$$

where λ_1, λ_2 represent the two wavelengths at which the signal intensity drops to half of its maximum value ($I_{\max} / 2$) [22]. Transmittance (T) is defined as follows:

$$T = |S_{21}|^2 \tag{3}$$

Here, S_{21} is the transmission coefficient.

The quality factor reflects how effectively the device stores energy relative to its rate of loss. A higher quality factor signifies sharper spectral features and reduced FWHM, which are essential for applications requiring precise wavelength discrimination, such as biosensing and optical filtering. For resonant systems such as plasmonic filters or waveguides, the quality factor is calculated using:

$$Q = \frac{\lambda_R}{FWHM} \tag{4}$$

where λ_R is the resonance wavelength [23].

IV. Results and Discussion

It is evident from Fig.(2a) the importance of careful mesh planning in engineering and physical simulations to achieve accurate results while minimizing computational costs, as it showed that the mesh was denser in the central part of the circle and gradually became less dense as the distance from the center increased. This indicated that the central region required higher precision due to the presence of complex geometric details and physical phenomena. Furthermore Fig.(2b) showed that the field intensity at both the first and second ports was high, indicating that this wavelength achieved high transmission (the wavelength is compatible with the filter design and satisfies the resonance condition). In contrast, in Fig.(2c), no light appeared at the second port, as the incident wave was almost completely reflected, which suggested high reflectivity and very low transmission (the wavelength, in this case, didn't match the filter design, and thus the resonance condition was not satisfied).

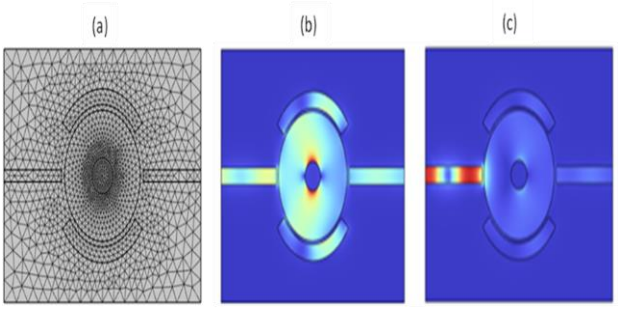

Fig:(2): a) finer meshing process, b) and c) electric field distributions at wavelength 750nm and 600nm respectively.

Fig.3: shows that as the value of *g* increased, both the transmittance and reflectance decreased, accompanied by an increase in absorptance. This occurred because of increasing in *g* values extended the optical path length within the material, enhancing the likelihood of light absorption, which in turn reduces transmittance and reflectance. Additionally, an increase in *g* resulted in broader peaks that became less sharp, with these peaks shifting forward. That happened due to the increasing in *g* led to reducing in the optical coupling between the filter elements, which in turn diminished the intensity of surface plasmonic resonance and consequently reduces the transmission efficiency.

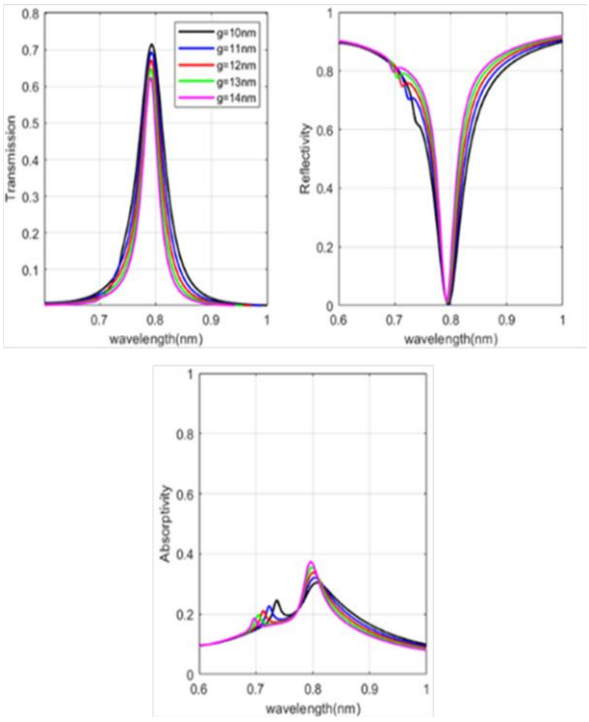

Fig:(3): transmission, reflectivity and absorptivity as functions of wavelength at different values of g.

Fig.4: illustrates the transmission as a function of wavelength for several values of the parameter d under two conditions of the parameter *L*. It was observed that as d increased, the peaks of the curves shifted to the right in both cases (*L*=175nm and 200nm). This shift indicates a geometrical effect caused by the increase in the thickness of the washer in the filter design. Additionally, the peak intensities decreased as *d* increased, which was attributed to the increased losses with the greater thickness of the washer. At *L*=200nm, the peaks were broader and taller compared to *L*=175nm, where the peaks were sharper. This difference suggests a change in the resonance frequency resulting from the altered geometrical design of the filter. The variation in transmission peaks with the thickness *d* and length *L* results from changes in the optical path and resonant conditions of the structure. Increasing *d* or *L* changes the effective refractive index and the resonance wavelength, which caused a redshift of the transmission spectra. This behavior has been realized in nanophotonic structures, where geometric parameters play a pivotal role in the wave-matter interaction.

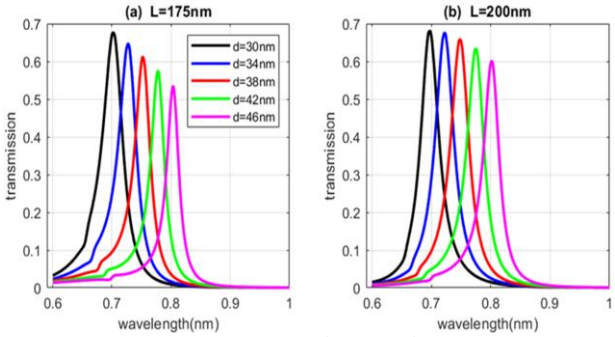

Fig:(4): transmission as a function of wavelength for different values *d* at *L*=175nm and *L*=200nm.

Fig.5: shows the transmittance as a function of wavelength for different values of *d* considering two cases of W_1. It was observed that in both cases, the peak intensities increased and the curve shifted to the right as *d* increased. However, at W_1= 30 nm, the spectral peaks were higher and broader compared to the case where W_1= 25 nm, Where the spectral peaks were lower and sharper. That was due to the relationship between *d* and the wavelength.

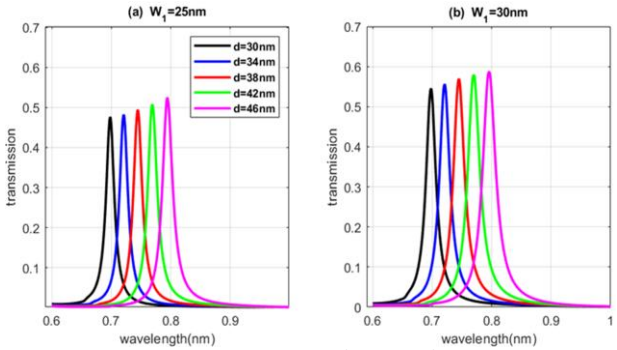

Fig:(5): transmission as a function of wavelength for different values *d* at W_1 =25nm and 30nm.

Fig.6: illustrates the transmission as a function of wavelength for various values of the *g* at two different values of the *L*. In both cases a significant decrease in the transmission peaks was observed as *g* increased. This is attributed to the fact that increasing the *g* reduces the interaction between surface plasmons, thereby decreasing the resonance intensity. Additionally, as *g* increased, the curves became less sharp and shifted slightly to the left. It was also evident that the transmission peaks in Fig.(6a) were lower compared to those in Fig.(6b), indicating a direct influence of the *L* on the resonance frequency.

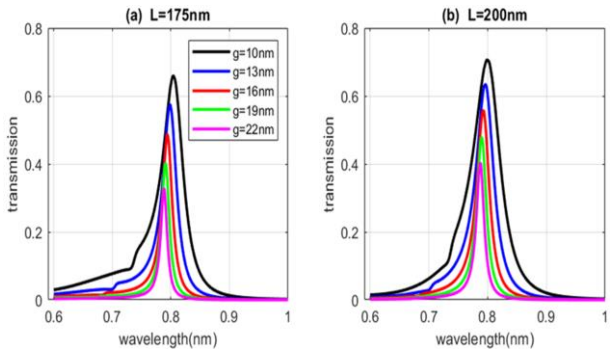

Fig:(6): transmission as a function of wavelength for different values *g* at *L*=175nm and *L*=200nm.

Fig.7: illustrates the transmission as a function of wavelength for different values of *g* and two distinct cases of the variable W_1. In both cases, it was observed that as *g* increases, the peak heights of the curves decreased significantly, accompanied by a noticeable shift of the spectrum toward shorter wavelengths (to the left). This behavior attributed to the increase in *g*, which reduced the optical coupling between the filter components, thereby decreasing the transmission. Furthermore, a comparison between the two cases showed in Fig.(7a) and Fig.(7b) It showed that when W_1 is smaller, the peak's heights are higher comparing to Fig.(7b), where the case is opposite.

This indicates that the effect of W_1 on transmission efficiency is relatively minor compared to the more pronounced impact of g.

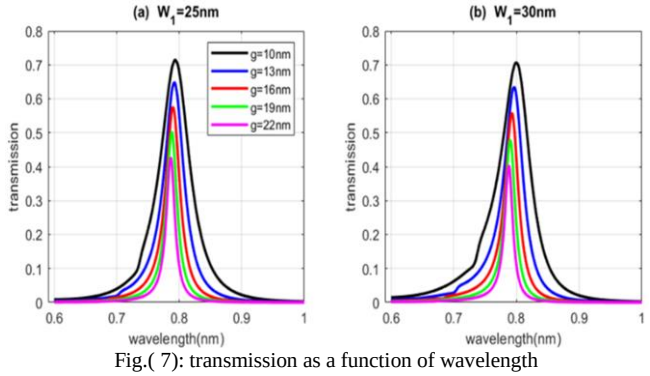

Fig.(7): transmission as a function of wavelength for different values g at W_1=25nm and W_1=30nm.

Fig.8: illustrates the FWHM, quality factor, and peak transmission as functions of the washer thickness d for three different values of L. In Fig.(8a), the FWHM decreased with increasing d for the low value of L=175nm, while for the higher values of L, the FWHM increased gradually with d until it reached a certain value, after which it starts to decreased. In Fig.(8b), the quality factor increased with increasing d for the low value of L=175nm. However, as L increased, the curve decreased with d until it reached a certain value, after which it began to rise up. In Fig.(7c), the peak transmission decreased with increasing d for the low value of L=175nm. When L=200 nm, the peak transmission started at a relatively high value and then decreased as d increased. For L=225nm, the peak transmission exhibited a curved pattern, initially increasing with d and then beginning to decline. This indicates that for each value of L, the filter exhibited a different response.

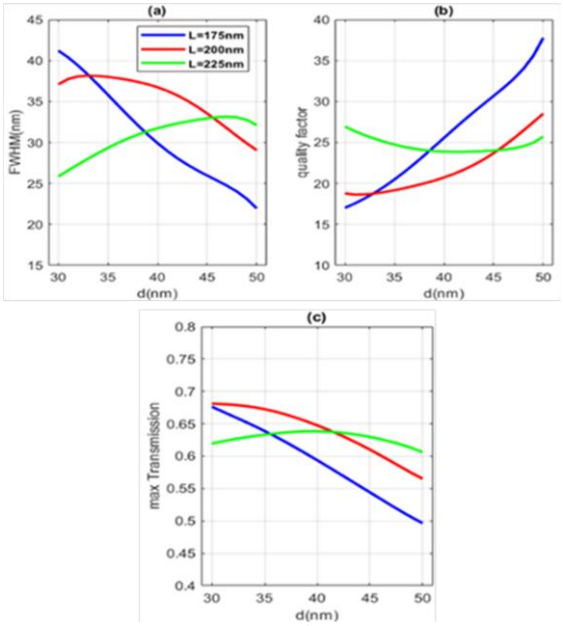

Fig:(8): FWHM, quality factor and maximum transmission as functions of d for three values of L.

Fig.9: illustrates the FWHM, quality factor, and maximum transmission as functions of the washer thickness for three different values of the variable W_1 while keeping the g fixed at 14 nm. In Fig.(9a), the FWHM increases with the washer thickness for all values of W_1. Furthermore, as W_1 increases, the curve shifts significantly upwards, indicating that the FWHM becomes larger with increasing W_1. In Fig.(9b), the quality factor for all W_1 values exhibited a curved behavior. It initially increased slightly with the washer thickness, but then it began to decrease as the thickness continued to grow. Additionally, the curve showed a notable downward shift with increasing W_1, signifying that the quality factor decreases as W_1 increases. In Fig.(9c), the maximum transmission increased slowly with the washer thickness at first then decreased gradually for all values of W_1. As W_1 increased, the curves shifted upward, indicating that the maximum transmission increases with larger W_1.

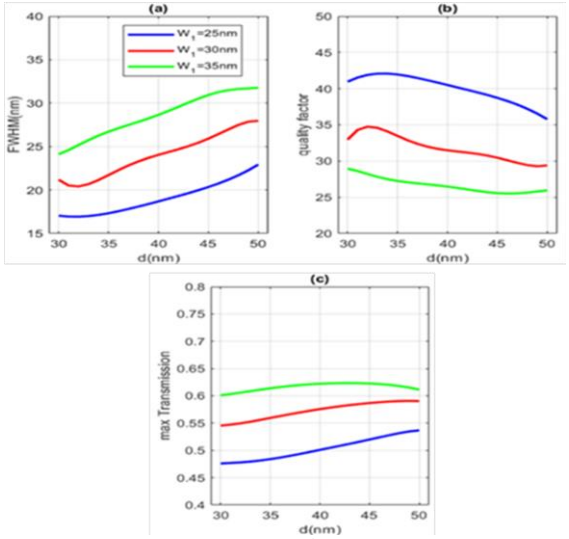

Fig.(9): FWHM, quality factor and maximum transmission as functions of d for three values of W_1.

Fig.10: illustrates the FWHM, quality factor, and maximum transmission as functions of d for three different values of the parameter of g. In Fig.(10a), it was observed that the FWHM increased with increasing d and decreased with increasing g. Conversely, in Fig.(10b), the quality factor decreased with increasing d and increased with increasing g. In Fig.(10c), the maximum transmission increased with increasing d and decreased with increasing g. This behavior can be attributed to the fact that increasing the gap thickness, g, weakens the interaction between the filter components, reducing losses and improving signal direction. Striking a balance between d and g is crucial to achieving optimal performance. A thicker gap reduces the interaction between the structure components, and then improving the quality factor by reducing the losses. Increase the parameter d led to maximum transmission, while increased the gap g yielded a reduction of transmission. It was vital to balance d and g for the best performance.

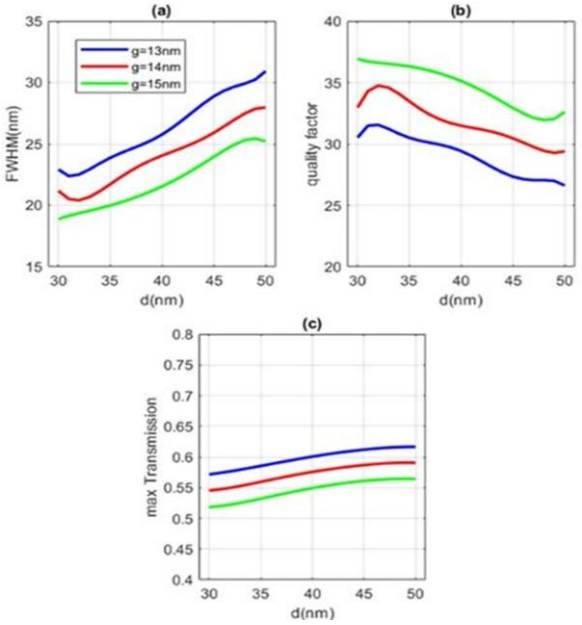

Fig:(10): FWHM, quality factor and maximum transmission as functions of *d* for three values of *g*.

Fig.11: illustrates the FWHM, quality factor, and maximum transmittance as functions of gap thickness for three values of the parameter *d*. In Fig.(11a), the FWHM increased with increasing of g for the all values of *d*. Moreover, as *d* increased, the curve shifted downward, indicating that the higher values of *d* resulted in lower FWHM. In Fig.(11b), the opposite trend was observed. The quality factor increased with increasing *g* for the all values of *d*. Additionally, as *d* increased, the curve shifted upward, meaning that higher values of *d* lead to a greater quality factor. In Fig.(11c), the maximum transmittance decreased linearly with increasing *g* for all values of *d*. Furthermore, as *d* increased, the curve shifts downward, indicating that higher values of *d* caused lower values of maximum transmittance.

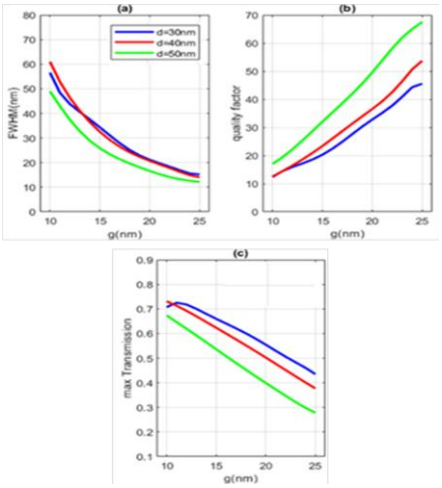

Fig:(11): FWHM, quality factor and maximum transmission as functions of *g* for three values of *d*.

Fig.12: illustrates the FWHM, quality factor, and maximum transmittance as functions of g for three values of r_1 parameter. In Fig. (12a), the FWHM decreased gradually with increasing in *g* values for the all values of r_1. As r_1 increased, the curve shifted slightly upward, indicating a minor increase in the FWHM with higher r_1. In Fig. (12b), the quality factor increased with increasing *g* for the all values of r_1. Additionally, as r_1 increased, the curve experienced a very slight initial decrease followed by a slight increase, indicating that the quality factor was affected by a subtle and non-uniform manner by variations in r_1. In Fig. (12c), a linear relationship was observed, where the maximum transmittance decreased with increasing *g* for the all values of r_1. Furthermore, as r_1 increased, the curve shifted slightly upward, suggesting that the maximum transmittance only minimally affected by higher values of r_1.

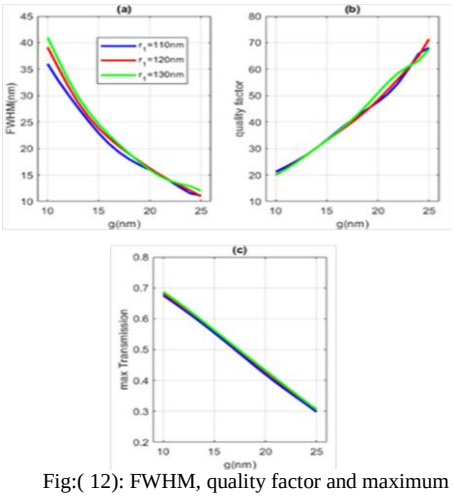

Fig:(12): FWHM, quality factor and maximum transmission as functions of *g* for three values of r_1.

Fig.13: illustrates the FWHM, quality factor, and maximum transmittance as functions of *d* for three values of the parameter W_2. In Fig.(13a), the FWHM at W_2 =25 nm increased significantly with increasing *d* until it reached a certain value, after which it began to decrease. However, for W_2=30 nm and W_2=35 nm, the FWHM decreased slightly at first, and then increased as *d* increased. In Fig.(13b), the opposite trend was observed. For W_2 =25 nm, the quality factor decreased with increasing *d* until it reached a specific value, and then slightly increased. For W_2 =30 nm and W_2 =35 nm, the quality factor initially increased slightly, then decreased with further increasing in *d* values. In Fig.(13c), the maximum transmittance increased with increasing of the *d* values for all values of W_2. The influence of W_2 on the curve was minimal, indicating only a very slight effect. This occurred because the variation range of W_2 was relatively small and didn't significantly alter the effective optical path length or resonance conditions within the filter structure. As a result, the transmission characteristics exhibited only minor changes, indicating that the device performance was relatively stable with respect to small perturbations in W_2.

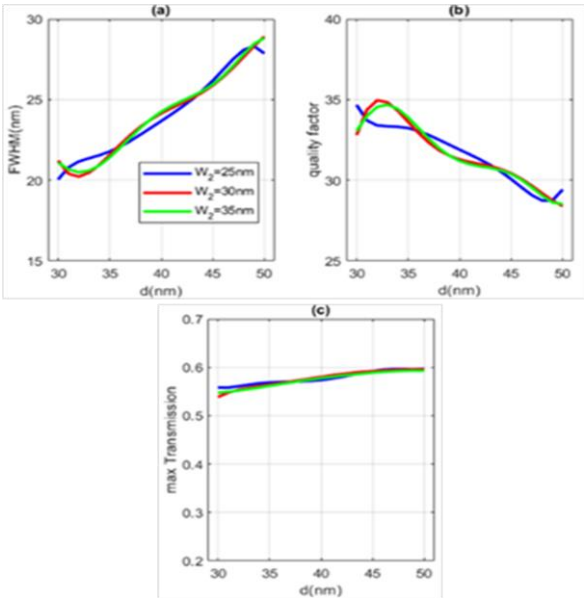

Fig:(13): FWHM, quality factor and maximum transmission as functions of d for three values of W_2.

Fig.14: illustrates the transmission as a function of wavelength for many values of d and using Drude model for Ag and Au. In both cases, we observed that as d increased, the peak heights gradually increased and shifted to the right. However, in Fig.(14a), the peaks were higher and sharper compared to Fig.(14b), where the peaks were lower and broader, indicating higher losses and lower selectivity.

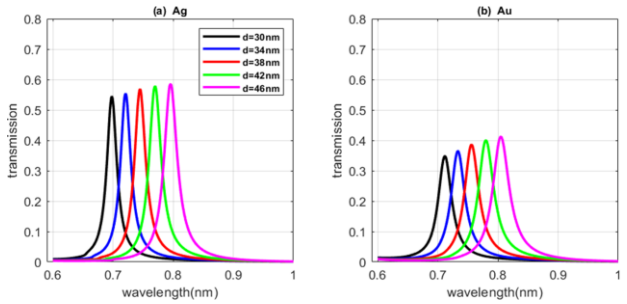

Fig.(14): transmission as a function of wavelength for different values of d and g=14nm using Drude model for: a) Ag and b) Au.

The performance tuning of a plasmonic filter was not governed by a single parameter such as FWHM, quality factor, or peak transmission but was instead a function of the collective contribution of all these metrics, depending on the intended application. The table presents a comparative analysis between various plasmonic filter designs and the one proposed in this work.

TABLE II. comparison of FWHM, quality factor and maximum transmission for many plasmonic filters.

FWHM (nm)	Quality factor	Maximum transmission %	Reference
45	35.27	80	[24]
10	47.7	82	[25]
13	62.79	N/A	[26]
N/A	95	99	[27]
10	70	75	proposed filter

V. Conclusions

The findings of this work demonstrated that altering the structural parameters specifically d and g had a significant impact on the spectral behaviors of transmission, reflection, and absorption. The results demonstrated that small geometric changes such as adjusting the washer width (d) or the gap (g) could markedly influence the transmission spectrum. Increasing the washer's width led to a redshift, indicating a stronger wave interaction, while increasing the gap weakened the resonance and shifted the peak toward shorter wavelengths. These behaviors highlight the structure's responsiveness to design variations.

Additionally, the type of used material played a major role in the performance of filters. Silver, for instance, exhibited higher transmission and sharper resonances compared to gold, making it more favorable for precise optical filtering. Overall, these findings emphasized the importance of optimizing both geometry and material to improve the filter's performance for different applications like sensing, wavelength routing, and integrated photonics.

Conflict of Interest

Authors declare that they have no conflict of interest

References

[1] M. ElKabbash, "Active Plasmonics and Metamaterials," Ph.D. dissertation, Dept. Physics, Case Western Reserve Univ., Cleveland, OH, USA, 2017.

[2] F. Ding and S. I. Bozhevolnyi, "A review of unidirectional surface plasmon polariton metacouplers," *IEEE J. Sel. Top. Quantum Electron.*, vol. 25, no. 3, pp. 1–11, 2019. doi: 10.1109/JSTQE.2019.2894067

[3] J. Zhang and L. Zhang, "Nanostructures for surface plasmons," *Adv. Opt. Photonics*, vol. 4, no. 2, pp. 157–321, 2012. doi: 10.1364/AOP.4.000157

[4] M. L. Brongersma and P. G. Kik, "Surface plasmon nanophotonics," vol. 131. Springer, 2007.

[5] G. Duffett, "Metal-insulator-metal nanoresonators for refractive index sensing," Ph.D. dissertation, Univ. of York, York, UK, 2021.

[6] S. M. Ebadi, S. Khani, and J. Örtegren, "Design of miniaturized wide band-pass plasmonic filters in MIM waveguides with tailored spectral filtering," *Opt. Quantum Electron.*, vol. 56, no. 5, pp. 1–24, 2024. doi: 10.1007/s11082-024-06732-w

[7] M. Babaie, M. Afsahi, and M. Danaie, "Plasmonic Metal–Insulator–Metal Filter and Refractive Index Sensor Based on Semi-Rings Coupled to a Disk Resonator," *Sens. Imaging*, vol. 26, no. 1, p. 100, 2025.

[8] M. Hasan *et al.*, "Plasmonic corrugated waveguide coupled to a rectangular nano-resonator as an optical filter," *OSA Contin.*, vol. 3, no. 12, pp. 3314–3323, 2020.

doi: 10.1364/OSAC.403762
[9] A. Ren *et al.*, "Emerging light-emitting diodes for next-generation data communications," *Nat. Electron.*, vol. 4, no. 8, pp. 559–572, 2021. doi: 10.1038/s41928-021-00624-7
[10] D. Liu, H. Xu, Y. Tan, Y. Shi, and D. Dai, "Silicon photonic filters," *Microw. Opt. Technol. Lett.*, vol. 63, no. 9, pp. 2252–2268, 2021. doi: 10.1002/mop.32509
[11] W. Feng, T. Qin, and X. Tang, "Advances in Infrared Detectors for In-Memory Sensing and Computing.," *Photonics*, 2024. doi: 10.3390/photonics11121138
[12] H. Yasser and M. Benhaliliba, "A Plasmonic Photonic Crystal Fiber Sensor with Simplified Features for Identifying Unidentified Analytes," *Univ. Thi-Qar J. Sci.*, vol. 11, no. 1, pp. 74–82, 2024. doi:10.32792/utq/utjsci/v11i1.1176
[13] V. Pareek, A. Bhargava, R. Gupta, N. Jain, and J. Panwar, "Synthesis and applications of noble metal nanoparticles: a review," *Adv. Sci. Eng. Med.*, vol. 9, no. 7, pp. 527–544, 2017. doi: 10.1166/asem.2017.2027
[14] J. Zhou, T. Yang, J. Chen, C. Wang, H. Zhang, and Y. Shao, "Two-dimensional nanomaterial-based plasmonic sensing applications: Advances and challenges," *Coord. Chem. Rev.*, vol. 410, p. 213218, 2020. doi: 10.1016/j.ccr.2020.213218
[15] V. N. Konopsky, "Long-range surface plasmons on duplex metal nanolayers," *Photonics Nanostructures-Fundamentals Appl.*, vol. 39, p. 100788, 2020. doi: 10.1016/j.photonics.2020.100788
[16] J. Homola, "Surface plasmon resonance sensors for detection of chemical and biological species," *Chem. Rev.*, vol. 108, no. 2, pp. 462–493, 2008. dio: 10.1021/cr068107d
[17] Z. Han and S. I. Bozhevolnyi, "Radiation guiding with surface plasmon polaritons," *Reports Prog. Phys.*, vol. 76, no. 1, p. 16402, 2012. doi: 10.1088/0034-4885/76/1/016402
[18] M. Dressel and G. Grüner, *Electrodynamics of solids: optical properties of electrons in matter*. Cambridge university press, 2002.
[19] J. Li, Z. Lou, and B. Li, "Nanostructured materials with localized surface plasmon resonance for photocatalysis," *Chinese Chem. Lett.*, vol. 33, no. 3, pp. 1154–1168, 2022. doi: 10.1016/j.cclet.2021.07.059
[20] N. L. Kazanskiy, S. N. Khonina, and M. A. Butt, "Plasmonic sensors based on Metal-insulator-metal waveguides for refractive index sensing applications: A brief review," *Phys. E Low-dimensional Syst. nanostructures*, vol. 117, p. 113798, 2020. doi: 10.1016/j.physe.2019.113798
[21] L. Wang, M. Hasanzadeh Kafshgari, and M. Meunier, "Optical properties and applications of plasmonic-metal nanoparticles," *Adv. Funct. Mater.*, vol. 30, no. 51, p. 2005400, 2020. doi:10.1002/adfm.202005400
[22] D. Fleischman, K. T. Fountaine, C. R. Bukowsky, G. Tagliabue, L. A. Sweatlock, and H. A. Atwater, "High spectral resolution plasmonic color filters with subwavelength dimensions," *Acs Photonics*, vol. 6, no. 2, pp. 332–338, 2019. doi: 10.1021/acsphotonics.8b01634
[23] Z. Zhang, J. Yang, Y. Han, X. He, J. Huang, and D. Chen, "Hybridization-induced resonances with high-quality factor in a plasmonic chipscale ring-disk nanocavity," *Waves in Random and Complex Media*, vol. 31, no. 6, pp. 2327–2336, 2021. doi:10.1080/17455030.2020.1742401
[24] I. Zegaar, A. Hocini, A. Harhouz, D. Khedrouche, and H. Ben Salah, "Design of a double-mode Plasmonic wavelength filter using a defective circular nano-disk resonator coupled to two MIM waveguides," *Prog. Electromagn. Res. Lett*, vol. 104, pp. 67–75, 2022. doi: 10.2528/PIERL22012905
[25] Z. Chen *et al.*, "Tunable high quality factor in two multimode plasmonic stubs waveguide," *Sci. Rep.*, vol. 6, no. 1, p. 24446, 2016. doi: 10.1038/srep24446
[26] J. Mao, X. Zhai, L. Wang, and H. Li, "Numerical analysis of near-infrared plasmonic filter with high figure of merit based on Fano resonance," *Appl. Phys. Express*, vol. 10, no. 8, p. 82201, 2017. doi: 10.7567/APEX.10.082201
[27] F. Abdolalipour and M. Pourmahyabadi, "High Q-factor plasmonic filter based on MIM structures and its application in the design of a dual band demultiplexer for optical communication wavelengths," *J. Opt. Soc. Am. B*, vol. 39, no. 1, pp. 364–372, 2021. doi: 10.1364/JOSAB.443140